

A Generalized Control Model and Its Digital Algorithm for Aerospace Electrohydraulic Actuators [†]

Shoujun Zhao *, Keqin Chen, Xiaosha Zhang, Yingxin Zhao, Guanghui Jing, Chuanwei Yin and Xiao Xue

Beijing Institute of Precision Mechatronics and Controls, No.1 South DaHongMen Road, Fengtai District, Beijing 100076, China; ckq0315@163.com (K.C.); zxs602wwyx@163.com (X.Z.); zyx_0@sina.com (Y.Z.); jingghhit@163.com (G.J.); yinchw_calt@163.com (C.Y.); xiaoxue_ht@163.com (X.X.)

* Correspondence: shoujunzhao@vip.sina.com; Tel.: +86-10-8852-0124

† Presented at the First International Electronic Conference on Actuator Technology: Materials, Devices and Applications, 23–27 November 2020; Available online: <https://iecat2020.sciforum.net/>.

Published: 20 November 2020

Abstract: It is difficult to describe precisely, and thus control satisfactorily, the dynamics of an electrohydraulic actuator to drive a high thrust liquid launcher engine, whose structural resonant frequency is usually low due to its heavy inertia and its complicated mass distribution. A generalized model is therefore put forward for maximum simplification and sufficient approximation, where a second-order transfer function is used to model the heavy mass-spring nature of the large engine body outside of the rod position loop, another second-order transfer function with two zeros and two poles representing the hydro-mechanical composite resonance effect in the closed rod position loop. A combined control strategy is applied to meet the stringent specification of static and dynamic performances, including a notch filter, a piecewise or nonlinear proportional, integral and differential (PID) controller and a feed-forward compensation. The control algorithm is implemented in digital signal processors with the same software structure but different parameters for different aerospace actuators. Compared to other approaches, this one makes it easier to grasp the system resonance nature, and, most importantly, the traditional dynamic pressure feedback (DPF) is replaced with the convenient digital algorithm, bringing prominent benefits such as a simplified design, reduced hardware cost and inherent higher reliability. The approach has been validated by simulation, experiments and successful flights.

Keywords: control model; control algorithm; electrohydraulic actuators

1. Introduction

The electro-hydraulic servo actuation is a well-developed technology. Nonetheless, most of its physical understanding and mathematical modeling have been referred to the Hydraulic Control Systems by H.E. Merritt as early as in 1967 [1]. In most cases, it was assumed that the driven load had sufficiently high structural resonances and was modeled as a lumped mass directly attached to the piston rod or motor shaft, with the hydraulic natural frequency dominating the control loop. However, in aerospace applications, such as rudders, fins and engines, due to weight and space limitations, the structural stiffness is usually low, and the model has to be modified. This was also discussed in the classic book, where, however, only the dynamics at the motor shaft point was elaborated, with the dynamics at the load end left open for more work [1] (pp. 157–162).

An appropriate model for realistic aerospace applications was presented by J.W. Edward for an aircraft rudder control servo system [2]. A spring was inserted as the structural compliance into the interface between the piston rod and the rudder. The structural natural frequency, the hydraulic

natural frequency and the derived composite hydro-mechanical natural frequency were clearly depicted and incorporated into the model, based on which the rudder surface dynamics was controlled by the Dynamic Pressure Feedback (DPF) method and matched well with the test results. The concise approach has been accepted so far [3] (pp. 35–37), but not widely enough, as seen by the author. In most current publications on electro-hydraulics, only the hydraulic resonance is included [4,5]. Furthermore, in most papers studying various emerging electro-hydrostatic actuators, where there are also hydraulic cylinders, only the hydraulic natural frequency is considered [6,7]. This approach might work well elsewhere but not in highly dynamic aerospace actuators. Moreover, since the digital control is the first choice nowadays, a better model is greatly helpful to understand the underlying physics, to fabricate the control algorithm and to accelerate the development process.

The author’s team has been working on electro-hydraulic actuators to gimbal Chinese non-toxic-non-pollution launcher engines [8–10]. In practice, the easy approach by J.W. Edwards has been used and developed with a new application perspective and more details, worthy of being elaborated here. For a variety of actuation systems, a normalized model was developed, in the easy form of a control block diagram written in transfer functions. A one-mass-one-spring model of the structural resonance, including the natural frequency and the damping ratio, as well as its measurement, was described. Inside the piston position loop, there was another second-order transfer function with two zeros and two poles representing the hydro-mechanical composite resonance effect. It was pointed out that the poorly damped and low frequency structural load resonance is the root cause of the poor system stability, rather than the hydraulic resonance, as mostly claimed. A combined control strategy of notch filter, nonlinear proportional, integral and differential (PID) controller and feed-forward compensation was given to meet the stringent requirement of static and dynamic performances. Another two-mass-two-spring model was introduced to deal with the thrust vector control of a heavy launcher engine with a more complex mass and stiffness distribution.

2. The System

A simplified schematics of an aerospace electrohydraulic actuation system to drive a launcher engine is described in Figure 1. The control loop includes a digital controller, a servo-valve, a double acting piston actuator and a linear displacement sensor imbedded inside the rod. The controller closes the negative feedback loop and performs digital algorithms for static and dynamic compensations. The expected output is the engine’s gimbaling angle. It is a classic aerospace design, where the feedback signal is picked up via the sensor inside the piston rod rather than via the angular output sensor.

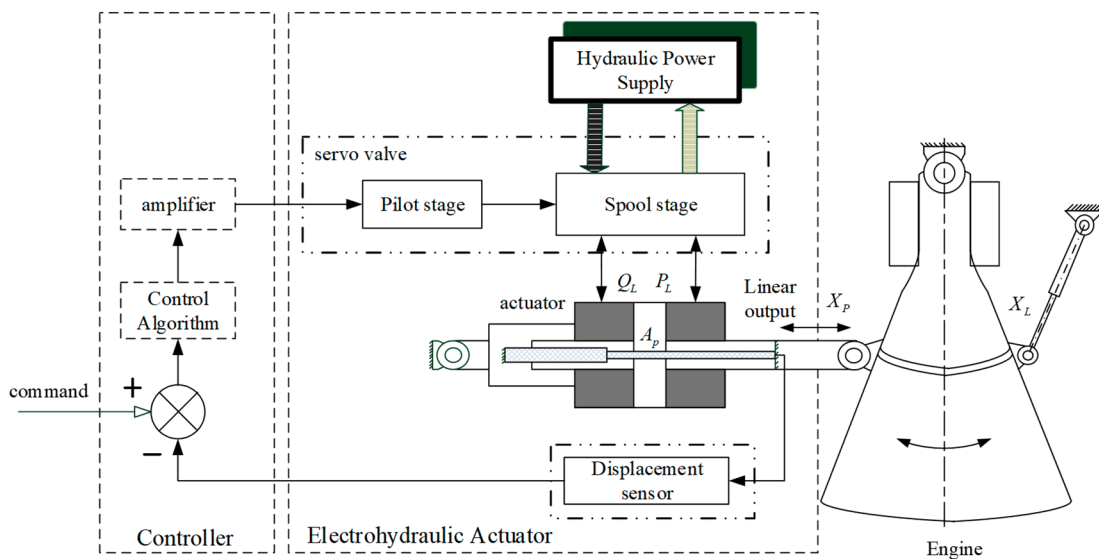


Figure 1. The simplified schematics for an aerospace electrohydraulic actuation system.

3. The System Model

The physical model to connect the actuator and the engine is critical. A one-mass-one-spring model is precise enough to depict most engine dynamics, as in Figure 2, since the gimbaling inertia is the dominating load.

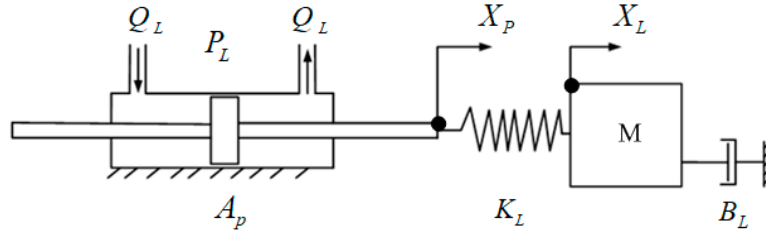


Figure 2. The physical model of a hydraulic actuator to drive an engine load.

Though its simplicity is a surprise, it is noteworthy that, in reality, there is neither a real connection spring between the rod and the engine nor a support spring at the actuator body end, even though a real spring exists in most load simulators. The model was found to precisely depict the internal mass distribution inside the engine body and hence its resonance dynamics. In practice, the system is designed in such a way that other structures, like the piston rod, the actuator body and its fixed supporting structure, are so strong that only the stiffness inside the load needs to be modeled.

Once the physics is clear, the mathematical equations are presented in Equations (1)–(4). The symbols are listed in Abbreviations.

$$Q_L = A_p \cdot S \cdot X_p + \frac{V_t}{4\beta} \cdot S \cdot P_L + K_c \cdot P_L \quad (1)$$

$$A_p \cdot P_L = K_L \cdot (X_p - X_L) \quad (2)$$

$$K_L \cdot (X_p - X_L) = M \cdot S^2 X_L + B_L \cdot S \cdot X_L \quad (3)$$

$$M = \frac{J}{R^2} \quad (4)$$

To derive a normalized model, the first step is that the load dynamics in Equation (3) has to be changed into a second-order transfer function, as in Equation (5).

$$G_L = \frac{X_L}{X_p} = \frac{1}{\frac{1}{\omega_L^2} S^2 + \frac{2\xi_L}{\omega_L} S + 1} \quad (5)$$

$$\omega_L = \sqrt{\frac{K_L}{M}} \quad (6)$$

$$\xi_L = \frac{B_L}{2K_L} \sqrt{\frac{K_L}{M}} \quad (7)$$

Note that the engine's structural resonant frequency ω_L and the damping ratio ξ_L are independent of any other electro-hydraulic actuator design, except for the installation geometry on which the rotation radius R depends. In ground testing, there are two measure points, one at the piston rod as X_p and the other at the engine gimbaling angular output as X_L . Usually, the engine gimbaling angle is measured in the form of linear displacement and converted to the angular value.

The next step is to represent Equations (1), (2) and (5) into a control block diagram, as in Figure 3.

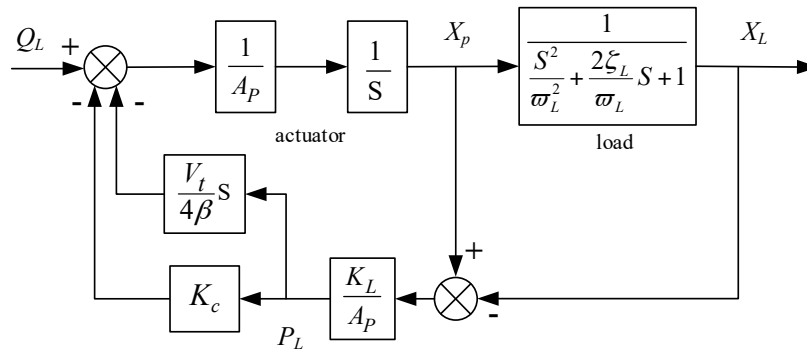


Figure 3. The block diagram of a hydraulic actuator to drive an engine load.

So far, the model derivation in Figure 3 has been a routine and usually stops here. To get a more concise form, it needs to eliminate the minor loops. Though a little tricky and laborious, it is worth seeing the result, in Figure 4, after successful block reductions. With the servo-valve and the controller added, as well as a lumped open loop gain, the final normalized system model is given in Figure 5.

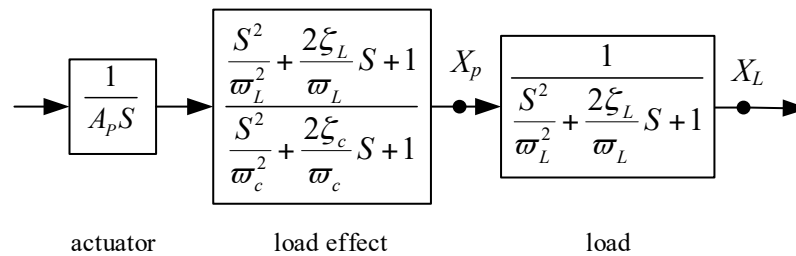


Figure 4. A normalized block diagram of a hydraulic actuator to drive an engine load.

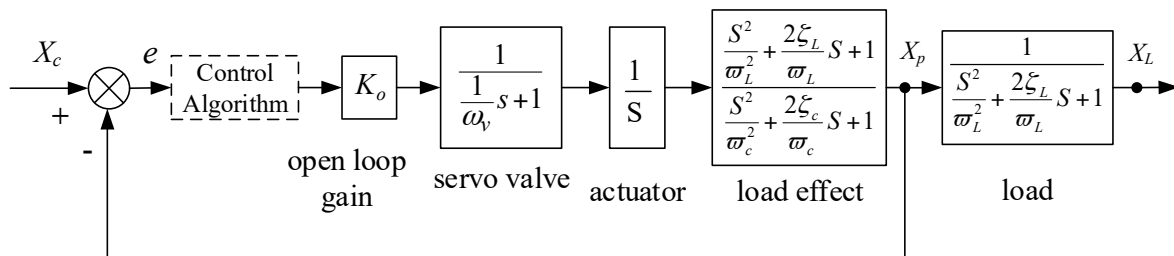


Figure 5. A normalized block diagram of an aerospace electrohydraulic actuation system.

The servo-valve is modeled as a first-order transfer function in that its bandwidth is chosen to be much higher than the structural resonance. The other underlying equations are given in Equations (8)–(12).

$$\omega_h = \sqrt{\frac{4A_p^2 \beta}{M V_t}} \tag{8}$$

$$\xi_h = \frac{K_c}{A_p} \sqrt{\frac{\beta M}{V_t}} \tag{9}$$

$$\frac{1}{\omega_c^2} = \frac{1}{\omega_L^2} + \frac{1}{\omega_h^2} \tag{10}$$

$$\xi_c = \left(\frac{\xi_L}{\omega_L} + \frac{\xi_L \cdot K_L}{\omega_L \cdot A_p^2} + \frac{\xi_h}{\omega_h} \right) \cdot \omega_c \tag{11}$$

$$K_o = K_{vi} \cdot K_{qi} \cdot K_{pd} \cdot \frac{1}{A_p} \tag{12}$$

As can be seen, for the expected output X_L , it is only a half-closed loop. Inside the piston position X_p loop, a second-order transfer function with two zeros and two poles dominates, both poorly damped, representing the hydro-mechanical composite resonance effect arising from the coupling between the load structural resonance and the hydraulic resonance, simply called “load effect”.

Since the structure natural frequency ω_L is low, the acting piston area A_p has to be large, so that the hydraulic natural frequency ω_h is much larger, often at least three times as large as ω_L . The resulted composite frequency ω_c in the denominator is a little smaller than the load natural frequency ω_L .

Inside the loop, the second-order numerator is helpful to cancel out the hydro-mechanical resonance effect of the second-order denominator. However, there is still another second-order denominator outside the loop, representing the load structural resonance. Therefore, both inside and outside the loop, there are two second-order denominators but only one second-order numerator. As a result, at least another second-order numerator is needed for the system’s stability. Without any compensation, a higher open loop gain would definitely lead to serious vibrations. In the real world, disastrous resonance would accompany the destruction of these structures.

In a word, the poorly damped and low-frequency structural load resonance is the root cause of the poor system stability, rather than the hydraulic resonance, as mostly claimed.

4. The Control Algorithm

A combined control strategy was developed as Figure 6.

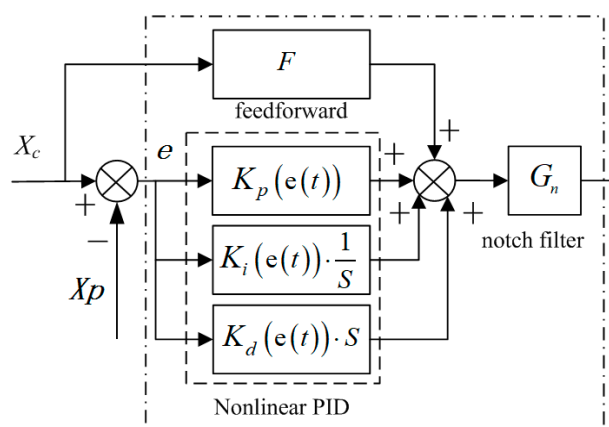


Figure 6. The combined control strategy.

The control algorithm comprises three parts: a notch filter, a nonlinear PID and a feed-forward compensation.

The notch filter function G_n is used to effectively suppress the system resonance, shown as Equation (13).

$$G_n = \frac{\frac{1}{\omega_{n1}^2} S^2 + \frac{2\xi_{n1}}{\omega_{n1}} S + 1}{\frac{1}{\omega_{n2}^2} S^2 + \frac{2\xi_{n2}}{\omega_{n2}} S + 1} \tag{13}$$

The rationale is that the poorly damped poles (ω_c, ξ_c) are cancelled out by a pair of nearly poorly damped zeros (ω_{n1}, ξ_{n1}) in the numerator and replaced with a pair of better damped poles (ω_{n2}, ξ_{n2}). It can be as simple as $\omega_{n1} = \omega_{n2} = \omega_c, \xi_{n1} = \xi_c, \xi_{n2} = 0.2\sim 0.4$, and usually $\xi_r \approx 0.03\sim 0.1, \xi_r \approx \xi_c + 0.01$. In practice, the parameters can be optimized to change the width and depth of the notch window.

The nonlinear PID is used to improve the tracking accuracy in the low frequency band, i.e., around 1~5 rad/s, with a piecewise proportional gain presented as Equation (14).

$$K_p(e(t)) = \begin{cases} f_K \cdot K_p & (f_K > 1) \quad |e(t)| \leq e_n \\ K_p & |e(t)| > e_n \end{cases} \quad (14)$$

A higher gain near zero is used to deal with the nonlinearities at the servo-valve spool center. The differential factor is usually small and helps to overcome the stiction forces in the system. As to the integral factor, it helps to improve the positioning precision and needs to be set as active only when the hydraulic power is on, so that an integration saturation and thus a jittering at the startup can be avoided.

A reduced-order feed-forward compensation is given as Equation (15).

$$F = K_f \cdot S \cdot X_c \quad (15)$$

In the intermediate frequency band, some distance from both the high frequency structural resonance region and the low frequency region, a higher open loop gain K_o is needed for high precision velocity tracking. However, even with a notch filter, there is a limit to increase the magnitude of K_o , e.g., one third of the structural natural frequency ω_c , so that a reduced-order feed-forward compensation is of great help to reduce the phase lag in this frequency region. The underlying principle is that, with higher and lower frequency components roughly neglected, there is only one integral transfer function left in the closed loop, which can be cancelled out by a differential counterpart represented as the feed-forward compensation.

As described above, with a combined control strategy, the system vibration due to structural resonance should be well suppressed while a satisfactory frequency response in the whole frequency region from low to high could be obtained.

5. Simulations and Experiments

An electro-hydraulic servo actuator to drive a high thrust liquid-hydrogen-liquid-oxygen launcher engine is illustrated here, with the main parameters shown in Table 1.

Table 1. The main parameters of the actuation system.

Parameter	Symbol	Value	Unit
Engine rotational inertia	J	1000	kg.m ²
Engine rotational arm	R	867	mm
Equivalent linear mass	M	1330	Kg
Engine natural frequency	ω_L	96	rad/s
Engine natural damping ratio	ξ_L	0.03~0.1	dimensionless
Actuator acting piston area	A	4082	mm ²
System pressure	Ps	21	MPa
Servovalve bandwidth (-45°)	ω_v	≥180	rad/s
Open loop gain	K_o	10~30	rad/s
Maximum angular output	-	4	degree
Digital Control Cycle	-	0.001	second

With only an open loop gain of 15 rad/s and without any other compensation, given a series of sinusoidal commands, the system was tested to study the load resonance effect, with bode plots of X_L and X_p shown in Figure 7.

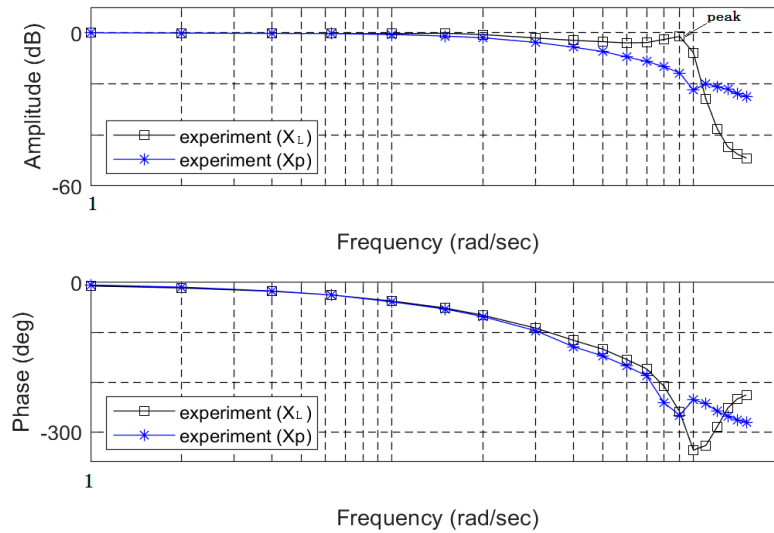


Figure 7. The dynamics of an uncompensated electro-hydraulic actuator and its engine load.

It is worth noting that, without compensation, with a small open loop gain, the system has a tendency to vibrate, as shown by the amplitude peak of the load response X_L . It is clear that the system has to be compensated for a bigger gain and better dynamics.

The engine’s structural resonance dynamics can be obtained by directly subtracting the response of X_p at the piston point from that of X_L at the load output in Figure 7, resulting in a curve shown in Figure 8, together with a simulation by a standard second-order transfer function.

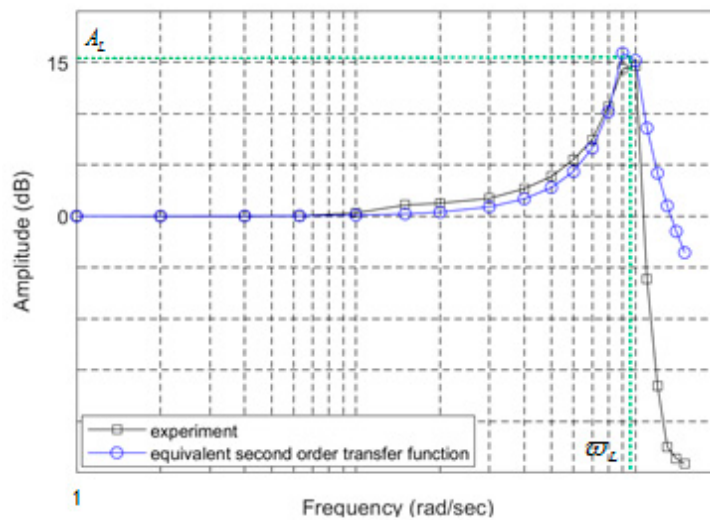


Figure 8. The structural dynamics of a liquid-hydrogen-liquid-oxygen launcher engine.

As shown, the load resonance can be modeled as a second-order transfer function with a sufficient precision. The structural natural frequency ω_L can be easily identified, while the natural damping ratio, ξ_L can be computed by Equation (16).

$$\xi_L = \frac{1}{2} 10^{-\frac{A_L}{20}} \tag{16}$$

As the peak amplitude shown is 15 dB, accordingly, the damping ratio ξ_L is 0.089.

To observe the hydro-mechanical resonance effect, we calculated the open loop response X_{po} by breaking the closed loop response X_p , with the method shown in Equations (17) and (18), where the response was represented in a complex form. The calculated bode plot is given in Figure 9.

$$C_{po} = \frac{C_p}{1 - C_p} \tag{17}$$

$$C_p = 10^{\frac{A}{20}}(\cos \theta + i \cdot \sin \theta) \tag{18}$$

It can be seen clearly that the hydro-mechanical resonance peak in the amplitude curve is the bottle neck to increase the stability margin. While the DPF was traditionally used to suppress the resonance, with the digital control at hand, a notch filter is the most straightforward and effective approach.

Also as in Figure 9, there are three regions marked to illustrate the combined control strategy. While the notch filter deals with the resonance in the high frequency region ①, a higher gain and the feed-forward compensation improve the velocity tracking precision in the intermediate frequency region ②, and the nonlinear PID upgrades the response in the low frequency region ③.

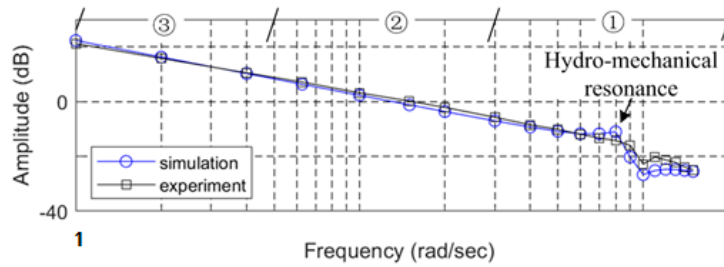


Figure 9. The open loop dynamics of the piston position loop.

With the combined control algorithm, the final compensated load frequency response X_L is shown in Figure 10, where the open loop gain was increased to 25 rad/s. The parameters in the PID and feed-forward compensation were optimized around the nominal point. The response data at the marked frequencies in Figure 10 are listed in Table 2.

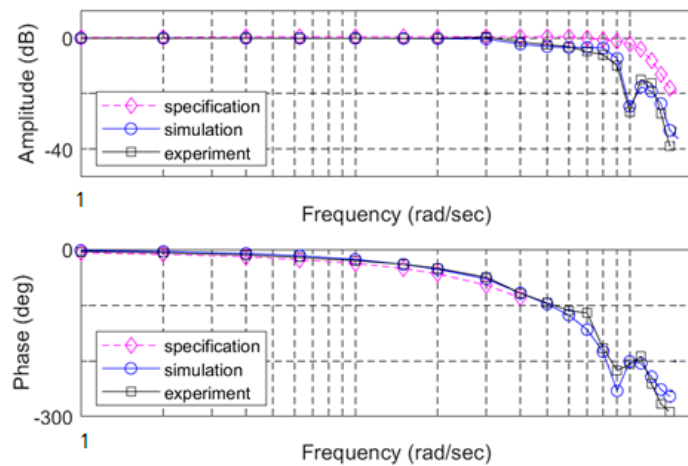


Figure 10. The final output dynamics of the compensated electro-hydraulic actuation system with a liquid-hydrogen-liquid-oxygen engine as load.

Table 2. The compensated load dynamic response at the marked frequencies.

Frequency (rad/s)	Amplitude (dB)	Phase (degree)
1	0.00	-4.03
2	0.00	-6.07
4	-0.02	-10.02
6.28	-0.10	-14.28
10	-0.05	-20.02
15	-0.06	-26.72
20	-0.08	-34.02
30	0.40	-49.86
40	-1.36	-78.36

50	-2.36	-96.05
60	-3.07	-109.89
70	-4.85	-114.13
80	-5.93	-177.13
90	-9.97	-217.44
100	-26.61	-206.48
110	-15.03	-192.02
120	-16.27	-240.83
130	-27.10	-277.58
140	-38.99	-291.92

6. A Modified Model and its Control Strategy for A More Complex System

While a one-mass-one-spring model is sufficient for most aerospace loads, there has to be some modifications for a high thrust liquid-oxygen-kerosene engine, since it has a more complicated mass and stiffness distribution [11]. It has two apparent structural natural frequencies, so that a two-mass-two-spring model has to be used. The tested structural dynamics was plotted and compared with the simulation in Figure 11. The two-mass-two-spring physical model is depicted in Figure 12.

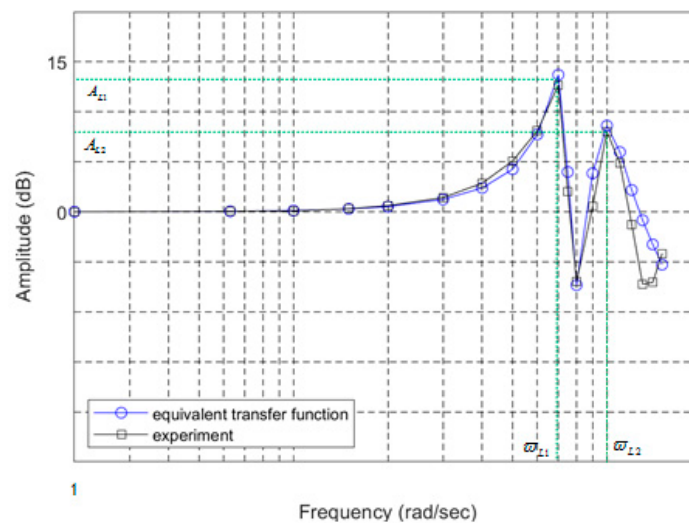


Figure 11. The structural dynamics of a liquid-oxygen-kerosene launcher engine.

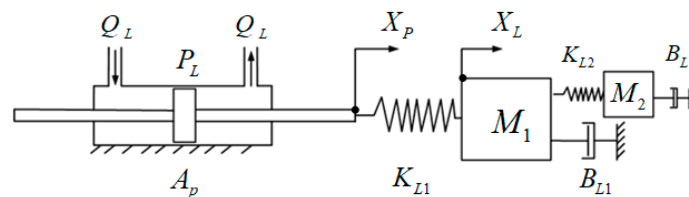


Figure 12. The physical model of a hydraulic actuator to drive a liquid-oxygen-kerosene engine.

The corresponding normalized system block diagram was derived as Figure 13, where there are representations similar to those in Figure 5 but with an additional structural resonance and an additional corresponding composite hydro-mechanical resonance. Since the two structural resonance frequencies are near each other, neither can be ignored, and both have to be treated with carefully.

As in the control algorithm, in Figure 6, two rather than one notch filter were used as Equation (19).

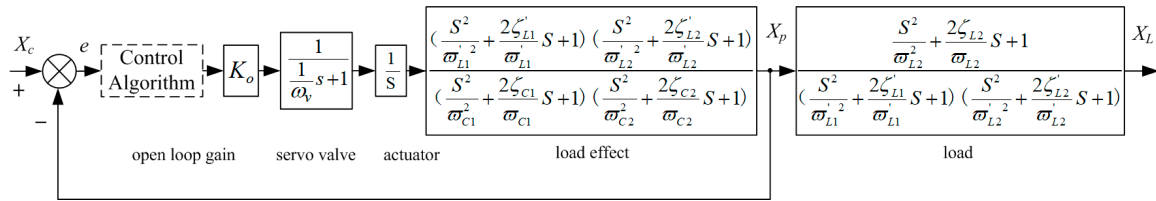


Figure 13. The normalized system block diagram to drive a two-mass-two-spring load.

Again, with the combined control algorithm, the satisfactory dynamics was obtained as shown in Figure 14.

$$G_n = \frac{\frac{1}{\omega_{n1}^2} S^2 + \frac{2\xi_{n1}}{\omega_{n1}} S + 1}{\frac{1}{\omega_{n2}^2} S^2 + \frac{2\xi_{n2}}{\omega_{n2}} S + 1} \cdot \frac{\frac{1}{\omega_{n3}^2} S^2 + \frac{2\xi_{n3}}{\omega_{n3}} S + 1}{\frac{1}{\omega_{n4}^2} S^2 + \frac{2\xi_{n4}}{\omega_{n4}} S + 1} \tag{19}$$

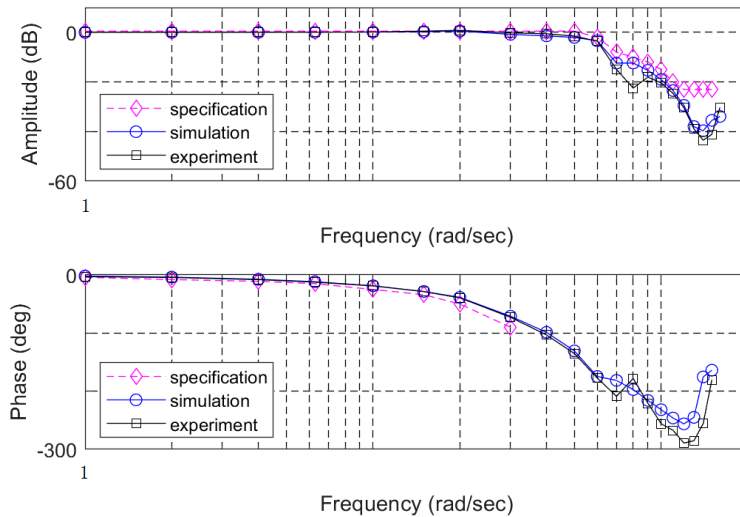


Figure 14. The final output dynamics of the compensated electro-hydraulic actuation system with a liquid-oxygen-kerosene engine as load.

7. Discussions

As shown above, unlike some applications where only the hydraulic resonance is cared, the load structural resonance cannot be ignored in an aerospace electro-hydraulic actuation system that needs to be as fast as possible. There is no reason why, in a highly dynamic actuator, the hydraulic natural frequency given by the design should be lower than that of the controlled target. Therefore, the load structural natural frequency becomes the lowest in the system and is the dominating design constraint.

One may argue that there should be no structural natural frequency ω_L part if the feedback is taken at the engine angular output point, as can be easily seen in Figures 4 and 5, in that it would be cancelled out. Nonetheless, there is the composite hydro-mechanical part left with the natural frequency ω_c . Because ω_c is derived from ω_L and ω_h , as in Equation (10), it is clear that the structural natural frequency ω_L is still the lowest and the ceiling to limit dynamics.

Since the demanded system bandwidth is approaching the structural natural frequency, a combined control algorithm has to be carefully designed, here comprising a notch filter to suppress the resonance in the high frequency region, a feed-forward compensation to improve the phase margin in the intermediate frequency region and a nonlinear PID to upgrade the performance in the low frequency region, respectively. Fortunately, a digital control approach was applied, and the seemingly complicated algorithm can be easily implemented in the software. In some applications,

even more complicated PID algorithms were used, e.g., an exponential proportional gain in the null region.

With the digital convenience, the parameters in the control algorithm can be defined to be changed easily, when different actuators or engines are used. With the same software package, a couple of actuation systems, e.g., to drive liquid-oxygen-kerosene engines and liquid-hydrogen-liquid-oxygen engines, have completed several flight missions.

Moreover, compared to the traditional DPF method in which electronic or hydro-mechanical devices to sense the differential pressures are needed, the digital approach is more effective, economical, flexible and reliable, due to the reduction of critical hardware.

Lastly, though in the presented systems servo-valves are used, the approach applies to pump-controlled systems in fast moving applications, i.e., electro-hydrostatic actuators (EHA), in which the hydraulic cylinders are used as well.

8. Conclusions

The load structural resonance was measured and represented clearly in a Bode plot. The concise second-order and fourth-order transfer function models were constructed, representing a one-mass-one spring model and a two-mass-two-spring model, respectively. A normalized system model was developed, comprising a closed loop for the piston displacement plus a load structural resonance outside. Inside the loop, the composite hydro-mechanical resonance was modelled and identified by the experiment. A combined control strategy was used to obtain satisfactory dynamic performances in the whole frequency range, from low to high. The experiment data matched well with the simulations, and satisfactory performances were obtained. It was demonstrated that, in a highly dynamic aerospace electro-hydraulic actuation system, the load structural resonance—rather than the hydraulic resonance, as often stated in other applications—is the dominating constraint and should be given priority in the design.

Author Contributions: S.Z. put forward the methods to measure the load structural resonance and constructed the framework of the normalized model and the control algorithm. K.C. conducted the simulation and experiments and decided the specifics of a feed-forward compensation. X.Z. built the original mathematical models and guided the simulation, experiments and substantiation of detailed control algorithms for a variety of actuation systems. Y.Z. optimized the model parameters of the structural dynamics and implemented the control algorithms for actuators to gimbal liquid-oxygen-kerosene engines. G.J. finalized the PID parameters and implemented the control algorithms for actuators to gimbal liquid-hydrogen-liquid-oxygen engines. C.Y. developed the all-factor optimization computer program for the control parameters and constructed the algorithm framework for digital signal processor based controllers. X.X. contributed to the data analysis and experiments. All authors have read and agreed to the published version of the manuscript.

Funding: This research received no external funding.

Acknowledgments: The research has been funded by the Chinese non-toxic-non-pollution launch vehicle programs. This paper publication is supported in part by the specific program “Manufacturing Basic Technology and Critical Components” of the National Key Research and Development Program of China (No. 2019YFB2005101).

Conflicts of Interest: The authors declare no conflict of interest.

Abbreviations

The following abbreviations are used in this manuscript:

DPF	Dynamic Pressure Feedback
PID	Proportional, Integral and Differential
EHA	Electro-hydrostatic Actuator

S	Laplace operator
Q_L	the loaded flowrate to the actuator
A_p	the acting piston area
X_c	the normalized command signal
X_p	the normalized piston position
X_L	the normalized load position output of the engine in the equivalent linear form
V_t	the total control volume of the two actuator chambers
β	the equivalent bulk modulus of the contained oil
P_L	the differential pressure across the piston
K_C	the lumped leakage coefficient across the piston, including that of the servovalve
K_L	the equivalent linear load stiffness
M	the equivalent moving load mass
B_L	the linear damping coefficient of the gimbaling engine
J	the rotational load inertia
R	the rotation radius of the load
ω_L, ξ_L	the structural natural frequency and corresponding damping ratio
e	the normalized position error between X_c and X_p
ω_h, ξ_h	the hydraulic natural frequency and corresponding damping ratio
ω_c, ξ_c	the composite hydro-mechanical natural frequency and corresponding damping ratio
$\omega_{L1}, \xi_{L1}, \omega_{nL2}, \xi_{L2}$	the first and second structural natural frequencies and corresponding damping ratios for a complex liquid-oxygen-kerosene engine
$\omega'_{L1}, \xi'_{L1}, \omega'_{L2}, \xi'_{L2}$	the first and second apparent structural natural frequencies and corresponding damping ratios for a complex liquid-oxygen-kerosene engine, derived from $\omega_{L1}, \xi_{L1}, \omega_{L2}, \xi_{L2}$
$\omega_{c1}, \xi_{c1}, \omega_{c2}, \xi_{c2}$	the two composite hydro-mechanical natural frequency and corresponding damping ratio for an electro-hydraulic actuation system to drive a complex liquid-oxygen-kerosene engine
ω_v	the first order servovalve frequency bandwidth
K_o	the nominal open loop gain of the piston position loop
K_{vi}	the volt-to-current conversion coefficient of the servovalve coil driver
K_{qi}	the nominal servovalve flow gain
K_{pd}	the conversion coefficient of the piston displacement sensor
K_p	the nominal proportional gain
K_i	the integral gain
K_d	the differential gain
f_k	the bigger proportional gain of the piecewise proportional gain
K_f	the feed-forward compensation gain
A	amplitude in the bode plot
θ	phase lag in the bode plot
C_p	the closed-loop frequency response of the piston position represented in the complex form
C_{p0}	the open loop frequency response of the piston position represented in the complex form
$\omega_{n1}, \xi_{n1}, \omega_{n2}, \xi_{n2}$	the compensation notch filter and its numerator and denominator frequencies and damping ratios, respectively
$\omega_{n1}, \xi_{n1}, \omega_{n2}, \xi_{n2}$	the 2nd compensation notch filter and its numerator and denominator frequencies and damping ratios, respectively;

References

1. Herbert, E. Merritt. Chapter V, Hydraulic Power Element. In *Hydraulic Control Systems*; John Wiley & Sons, Inc.: Hoboken, NJ, USA, 1967.
2. Edwards, J.W. *Analysis of an Electro-Hydraulic Aircraft Control Surface Servo and Comparison with Test Results*; NASA Technical Note, NASA TN D-6928; NASA: Washington, DC, USA, 1972.

3. Rydberg, K.E. *Hydraulic Servo Systems. IEI/Fluid and Mechanical Engineering Systems*; TMHP51 Fluid and Mechanical Engineering Systems, Linköping University: Linköping, Sweden, 2008.
4. Lazić, D.V.; Ristanović, M.R. Electrohydraulic thrust vector control of twin rocket engines with position feedback via angular transducers. *Control Eng. Pract.* **2007**, *15*, 583–594.
5. Mohit Law. Design Guidelines for an Electro-Hydraulic Actuator to Isolate Machines from Vibrations. In Proceedings of the 6th International & 27th All India Manufacturing Technology, Design and Research Conference (AIMTDR-2016), College of Engineering, Pune, Maharashtra, India, 16–18 December 2016.
6. Li, Y.; Jiao, Z.; Wang, Z. Design, Analysis, and Verification of an Electro-Hydrostatic Actuator for Distributed Actuation System. *Sensors* **2020**, *20*, 634, doi:10.3390/s20030634.
7. Li, Z.; Shang, Y.; Jiao, Z.; Lin, Y.; Wu, S.; Li, X. Analysis of the dynamic performance of an electro-hydrostatic actuator and improvement methods. *Chin. J. Aeronaut.* **2018**, *31*, 2312–2320, doi:10.1016/j.cja.2018.03.014.
8. Zeng, G.; Zhang, X. A TVC system for liquid oxygen-kerosene launch vehicle. In Proceedings of the 57th International Astronautical Congress, IAC-06-C4.1.06, Hyderabad, India, 24–28 September 2006.
9. Zhao, S.; Zhao, Y.; Zhang, X. The TVC Systems for a Chinese Liquid Oxygen and Kerosene Launch Vehicle, IAC-13-C4,P,27.p1. In Proceedings of the 64th International Astronautical Congress (IAC), Beijing, China, 25–29 October 2013.
10. Jing, G.; Zhang, X.; Zeng, G.; Zhao, S.; Yin, C. A Hydrogen-Turbopump-Powered Thrust Vector Control Servo System for High Thrust LH2/LOX Rocket Engines, IAC-17-D2.5.10. In Proceedings of the 68th International Astronautical Congress (IAC), Adelaide, Australia, 25–29 September 2017.
11. Yin, C.; Zhao, S.; Chen, K. The Algorithm Optimization Study on the Thrust Vector Servo Control for a Rocket Engine with Two Resonant Frequencies (in Chinese). *Rocket Launch Veh. Technol.* **2013**, *1*, 21–26.

Publisher’s Note: MDPI stays neutral with regard to jurisdictional claims in published maps and institutional affiliations.



© 2020 by the authors. Licensee MDPI, Basel, Switzerland. This article is an open access article distributed under the terms and conditions of the Creative Commons Attribution (CC BY) license (<http://creativecommons.org/licenses/by/4.0/>).